BISTATIC SCATTERING FROM BURIED TARGETS IN SHALLOW WATER

HENRIK SCHMIDT
Massachusetts Institute of Technology
Cambridge, MA 02139, USA

Abstract

The development of new concurrent detection and classification concepts has the potential of dramatically increasing the coverage rate of shallow water mine countermeasures, in particular for buried targets. The GOATS'98 experiment had as one of its main objectives to explore the possibility of basing such a concept on the measurement of classifying features of the 3-D acoustic scattering by such objects, using bistatic configurations made possible by the emerging autonomous underwater vehicle technology. Using an extensive suite of fixed and mobile mono- and bistatic acoustic arrays, the experiment produced an extraordinarily rich data set, which as described elsewhere in this volume is being extensively used for a variety of MCM-related issues, including mono- and bistatic synthetic aperture processing and subcritical seabed penetration physics. The analysis has revealed a number of unexpected acoustic phenomena in regard to the subcritical excitation of elastic waves in buried shells, and their radiation back into the water column. For example, a strong, delayed maximum in the bistatic scattering from a flush-buried spherical shell is observed at frequencies an order of magnitude higher than predicted for simple point-targets at the same burial depth. The OASES-3D target modelling framework is being used to investigate this phenomenon, and this paper describes some preliminary results, which demonstrate that full wave theory modelling is necessary to adequately describe scattering of evanescent waves from seabed targets. Thus, the traditional plane-wave, ray-tracing approach to the propagation to and from the target is demonstrated to be totally inadequate, and must be replaced by a scattering model incorporating a wide spatial spectrum of scattered propagation angles. The analysis also shows that although this scattering mechanism also exists for monostatic geometries, its bistatic enhancement is much stronger than the 'geometric', evanescent scattering. In addition, being due to the excitation of structural waves, the presence of this scattered component can potentially be applied for classification.

1. Introduction

High coverage rate is critical to operational mine countermeasures (MCM) detection and classification. Classical MCM sonar systems operate at high frequency, typically 30+ kHz to provide a resolution adequate for the acoustic imaging that is the basis for target classification. Except for a few pathological cases, the environmental acoustics does not allow these sonars to detect targets completely buried in the seabed at standoff ranges beyond critical, which for typical seabeds amounts to a few times the sonar altitude. This in turn severely limits the coverage rate of such systems against buried mines.

The Generic Ocean Array Technology Sonar (GOATS) concept uses a fleet of small Autonomous Underwater Vehicles (AUV) cooperating in a volumetric mapping of the acoustic scattering from proud or buried targets. It is specifically aimed at expanding the coverage rate for shallow and VSW MCM by performing concurrent detection and classification of proud and buried targets, exploring the unique 3-D spatial and temporal features of low- to mid-frequency target scattering. A potential application of GOATS is

illustrated in Fig. 1. One AUV insonifies the VSW seabed from off-shore with a powerful mid-frequency source such as a parametric sonar. The scattered field is measured by a formation of small AUVs equipped with acoustic arrays. The data are pre-processed and transmitted via a high-bandwidth communication capability to the master vehicle where the data from the multiple receiver platforms are combined to create a seabed image, as well as a 3-D map of the target scattering, which then forms the basis for both detection and classification.

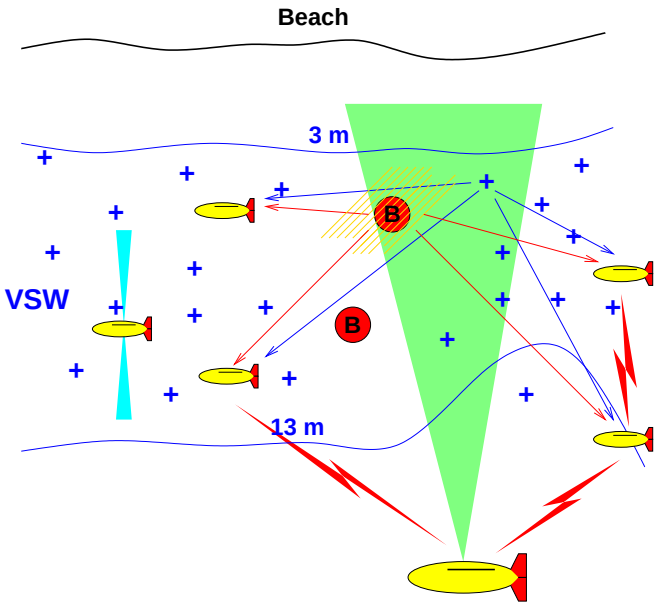

Figure 1 *GOATS concept for concurrent detection and classification of seabed targets using a network of autonomous underwater vehicles for forming a multi-static synthetic aperture. The master vehicle is insonifying the seabed from off-shore, connected with the receiver vehicle network using a high-bandwidth communication and navigation network. The multi-static synthetic aperture processing is applied for detection while the mapping of the 3-D scattered field is used for classification.*

There are several fundamental scientific and applied technology issues that must be resolved before the MCM performance of the GOATS concept can be evaluated. Among these unresolved issues are characterization of the mid-frequency (1-10 kHz) insonification regime, extension of sonar processing techniques to bi- and multi-static scenarios and optimization of information processing for the robust detection and classification of man-made objects. The use of the mid-frequency regime is of necessity for adequate bottom penetration [1], but it also provides additional information for classification by exciting frequency-dependent responses of the target. Bi- and multi-static scenarios complicate the data processing significantly, but they also increase the survey coverage rate and provide additional target information by measuring aspect-dependent responses of the target. Both of these results can be regarded as forms of data diversity, which may be used as an aid in cases where traditional high-frequency monostatic imaging fails. In sonar applications, there has been relatively little study of alternative techniques for buried target classification, although some laboratory-based studies have shown promise [2], [3], [4]. Data diversity techniques have been effectively employed in the buried land mine case [5] [6], where, as in the underwater case, the imaging wavelength is on the order of the target size.

This paper describes the results of a modelling and analysis effort regarding the fundamental scattering physics of buried targets, with particular focus on the interplay between the evanescent lateral wave fields in the sediment at subcritical angles, and structural waves in the target.

2. GOATS'98 bistatic imaging experiment

During the bistatic imaging phase of the GOATS'98 experiment, a stationary source was used to insonify a patch on the seafloor that contained a known target field (Fig. 2). The source used was a Topographic Parametric Sonar (TOPAS), which provides a highly directive beam on a given patch of the seafloor. A receiver array mounted on an autonomous underwater vehicle was used to sample the scattered field. The experiment was performed in an area close to shore with water depth 14 m and a sandy seabed. The sound velocity profile of the water column was a nearly uniform 1520 m/s.

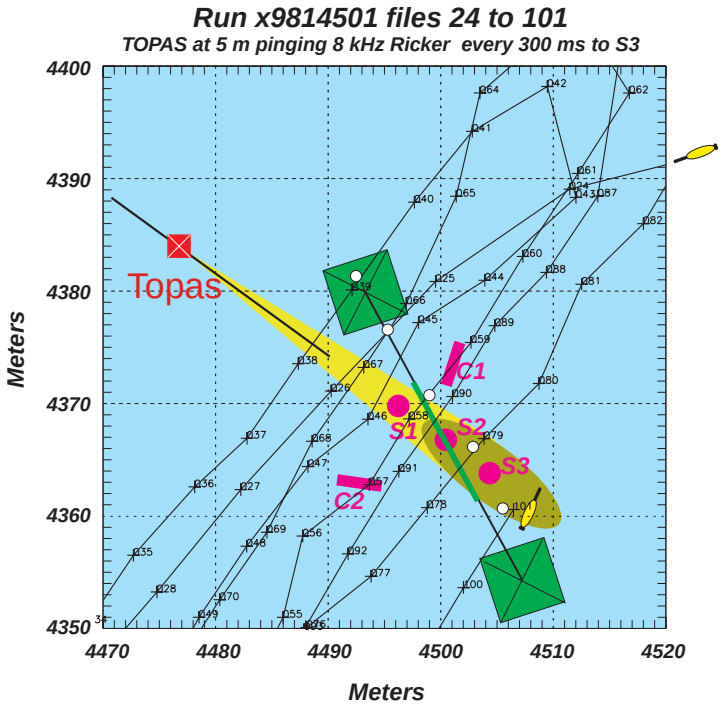

Figure 2 *GOATS'98 experimental geometry. A TOPAS parametric source is mounted on a tower, which may be relocated along a horizontal rail to change angles of incidence on the seabed targets. A fixed 128-element horizontal hydrophone array was suspended 5 m over the targets for fixed bistatic measurements, while an AUV equipped with a receiving array and acquisition system was used as a moving receiver platform, creating synthetic apertures at different offsets from the target field.*

2.1 Source

The TOPAS sonar is a parametric source with a secondary frequency band of 2–16 kHz. The source level in the secondary frequency band is 201 dB *re* μ*Pa* @ 1 *m*. This relatively low frequency band was chosen for improved seabed penetration, which in turn enhances the buried target detection capability. Although reduction in frequency obviously increases penetration at super-critical angles, the more interesting regime for rapid mapping is sub-critical insonification, which has been shown to provide significant evanescent wave field penetration in this frequency range [7]. The source transmitted a series of pings at a repetition period of 300 ms, with each ping being a broadband Ricker wavelet with centre frequency 8 kHz.

As illustrated in Fig. 2, the parametric projector was mounted on a 10 m tall tower that could be re-positioned along a 20 m long rail on the seabed to allow target insonification at grazing

angles below as well as above the critical angle of approximately 24° for penetration into the seabed [7]. During the experiment, both sub- and super-critical insonification angles were tested, but the current work concerns only sub-critical grazing angles.

2.2 Target field

Five targets of various geometry and burial conditions were deployed in a relatively smooth portion of sandy seabed, in an area 10 - 20 meters from the end of the TOPAS rail, as shown in Fig. 3. The targets included 3 air-filled spherical steel shells with diameter 1 m and wall thickness 3 cm. One was half-buried (S3), one flush-buried (S2), and one was buried 0.9 m below the surface (S1) at its centre. In addition 2 steel cylinders were flush-buried at aspect angles of 90° (C1) and 45° (C2) respectively. The 2 m long and 50 cm diameter cylinders were both water-filled and had a shell thickness of 6 mm.

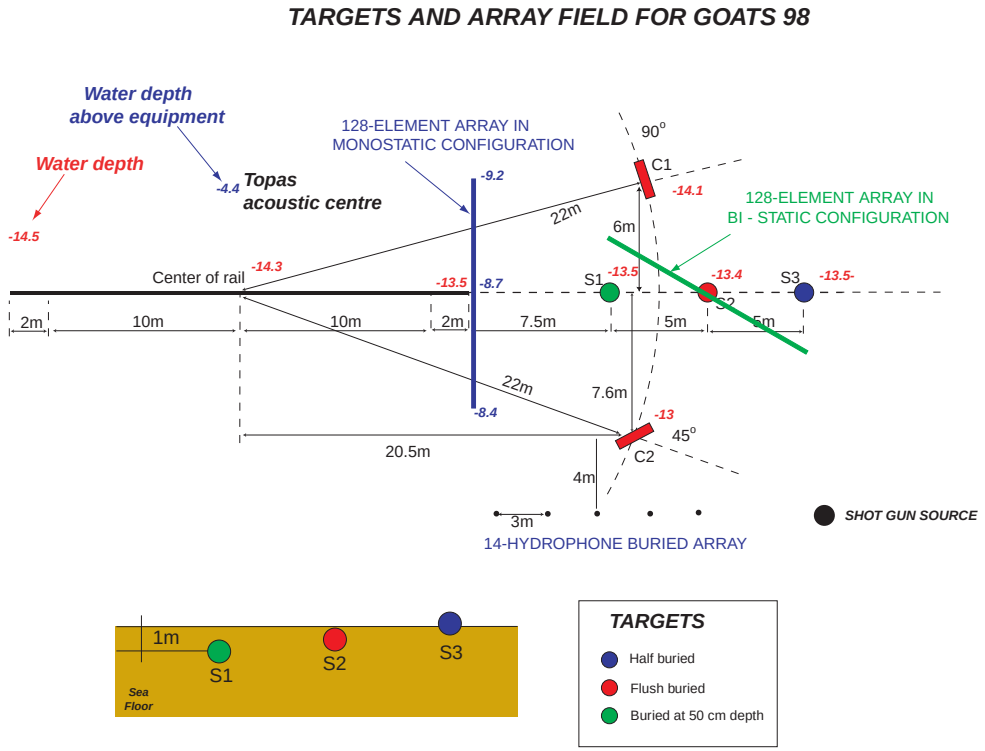

Figure 3 *Layout of the target field for GOATS'98. 5 targets were deployed, three empty spherical shells, half-buried (S3), flush-buried (S2) and completely buried (S1), respectively. In addition two water-filled cylindrical shells were flush buried, at aspects 90° (C1), and 45° (C2), respectively. The targets were deployed such that they could be insonified at angles above and below the critical grazing angle of approximately 24°. Here the horizontal line array is shown in a quasi-monostatic configuration.*

2.3. Autonomous Underwater Vehicle

The AUV used as a receiver platform was an Odyssey II AUV equipped with a linear acoustic array in a 'swordfish' configuration, as can be seen in Fig. 4. The array consisted of 8 omnidirectional hydrophones linearly spaced with $\Delta x = 0.1\ m$, which corresponds to the $\lambda/2$ sampling at 7.5 kHz. The apparent undersampling is mitigated by the fact that the array is not required to steer over the full 180 degree half-space.

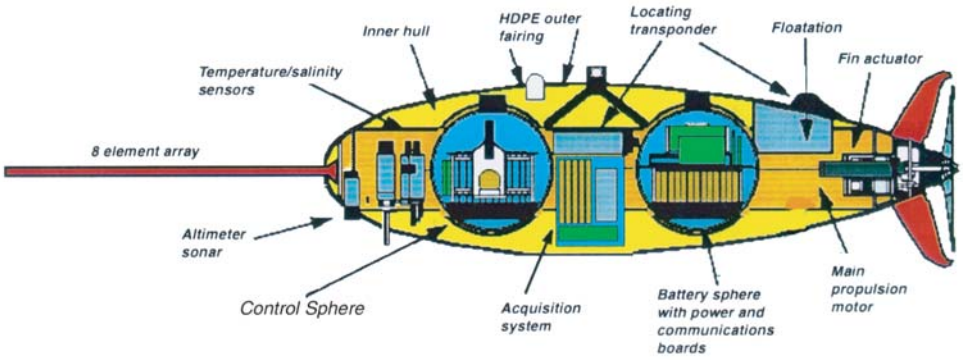

Figure 4 *Odyssey II AUV equipped with an 8-element array in a 'swordfish' configuration. The element spacing is 10 cm. A dedicated acquisition system is mounted in the centre bay of the vehicle, with data stored on disk for post-processing.*

The AUV was programmed to perform a 'lawn-mower' survey over the target field, with one of the legs shown in Fig. 2. The AUV was navigated using a 8-12 kHz long baseline (LBL) acoustic navigation system to travel between way-points alternating between the two sides of the target field. It used the LBL to update its position and adjust the trajectory every 10 seconds. The numbers on the AUV track indicate the vehicle position when the LBL navigation cycle was initiated. The navigation cycle was interleaved with the TOPAS transmissions to avoid mutual interference. To synchronize the transmissions with the navigation cycle, the LBL interrogation pulse was detected by the TOPAS receiver electronics, triggering a 7 second ping sequence after a 3 second delay. Thus, only 7 seconds of data were available for SAS processing in each navigation cycle, corresponding to a 7 m synthetic aperture.

3. Target scattering model

Using a 3-D adaptation of the approach of Ingenito [8], the target is represented by a *virtual source* with a radiation pattern determined by convolving the incident field by a target scattering function. The present 3-D implementation is very similar to the one recently presented by Makris [9], who rigorously derived the Fourier-Hankel representation of the 3-D waveguide field for a finite size spherical target, and then formally investigated the validity of representing the target as a *point scatterer*. Here, instead, the point-scatter assumption is directly adopted and the Fourier-Hankel transform of the scattered field is performed numerically, in a form which is directly compatible with the OASES infrastructure, totally consistent with the handling of rough interface scattering. In this *single-scattering* approach, the stratification is ignored in the actual scattering process, with the target assumed to be in an infinite medium. Thus, for an incident plane wave of wavenumber k_r and horizontal azimuthal angle θ_0, the target scattering is represented by a *shaded point s*ource term [8],

$$\chi(R,\theta,q_r) = \frac{\exp jkR}{R} S^{\pm}(\theta,q_r,\theta_0,k_r), \tag{1}$$

where $S^{\pm}(\theta,q_r,\theta,k_r)$ is the scattering function, with the $\pm$ representing the up- and downward propagating components. The scattering function is represented in terms of the horizontal wavenumbers k_r and q_r of the incident and scattered field, respectively, instead of

the more common representation in terms of vertical angles. However, using the wavenumber form we can directly obtain the scattering function for evanescent incident and scattered field components by analytical continuation, which is crucial to the modelling of scattering by buried targets.

For simple objects the scattering function can be determined analytically. Thus, for spheres, the expansion of the scattering function in terms of spherical harmonics is well established [8]. The scattering function in the evanescent regime $q_r\, k_r > k$ is handled by simple analytical continuation. For general targets the scattering function can be determined numerically, e.g. using finite-element approaches [10].

For a target in a stratified waveguide, Eq. (1) must be transformed into a wavenumber integral representation to be able to express the boundary conditions in the wavenumber domain [11]. For the point source, corresponding to the $\exp(jkR)\ /\ R$ term in Eq. (1), this transformation is provided by the *Sommerfeld-Weil* integral, with the kernel $j\ \exp(j\ q_z\ |\ z - z_t\ |)\ /\ q_z$ at depth z [12]. Applying the *stationary phase* or *far-field* approximation, the corresponding wavenumber kernel for the scattered field is achieved by simply shading the kernel of the Sommerfeld-Weil integral by the scattering function,

$$\tilde{\chi}\ell(z, \theta, q_r) = j\, \frac{e^{jq_z|z-zt|}}{q_z}\, S^{\pm}(\theta, q_r, \theta_0, k_r). \tag{2}$$

The wavenumber integral representation of the target scattering then follows as

$$\begin{aligned} \tilde{\chi}\ell(r, z, \theta) = \sum_{m=0}^{\infty} \begin{Bmatrix} \cos m\theta \\ \sin m\theta \end{Bmatrix} \int_0^{\infty} dq_r q_r J_m(q_r r) \\ \times\, j^{m+1} \frac{e^{jq_z|z-z_t\ |}}{qz}\, \tilde{S}_m^{\pm}(q_r, \theta_0, k_r) \end{aligned} \tag{3}$$

where $j^m\ S_m^{\pm}(qr, \theta 0, k_r)$ is the Fourier-Hankel transform of the scattering function in Eq. (2). The wavenumber representation of the discontinuity in pressure and particle velocity above and below the nominal target depth z_t, associated with the wavenumber kernels are then given by

$$\tilde{\chi}m;\, \ell(q_r, z) = j\, \frac{e^{jq_z|z-z_t\ |}}{q_z}\, \tilde{S}_m^{\pm}(q_r, \theta_0, k_r) \tag{4}$$

For incident fields of finite spectral width, the scattering function in Eq. (4) is replaced by an integral over the incident wavenumber k_r of the scattering function weighted by the spectral density of the incident field, with the sub-critical evanescent regime handled by simple analytical continuation, corresponding to complex incident angles θ_0. The resulting integral representation then is equivalent to a spatially shaded virtual point source, and the waveguide field can be directly computed using 3-D wavenumber integration [13].

The validity of the single-scattering approach for targets near interfaces is obviously at issue, but as shown by Fawcett [14] the approach appears sufficiently accurate for objects buried in sedimentary bottoms. However, the single-scatter approximation may be inadequate when

modelling the temporal details of the scattered signals. Here the late multiples may be of lower amplitude than the primary response, but separated enough in time to provide important classification information. Another related issue, in particular for objects close to the seabed interface, is the treatment of the target as a *point scatterer* which is a key feature of this approach. The validity of this approximation was rigorously addressed by Makris [9] who concluded that the point scatterer approximation for the sphere is valid for ranges in excess of a sphere diameter from the centroid. It is uncertain how this translates to the handling of transmission through the seabed interface from shallow-buried targets. However, it is hypothesized that by including the evanescent components of both the incident and scattered fields, the correct physics of the primary interaction with buried targets is adequately represented, at both super- and sub-critical sonar scenarios. In any case, all the approximations made here must ultimately be assessed by comparison to results of 'exact' numerical models and, more importantly, experiments such as GOATS'98.

4. Subcritical scattering by flush-buried sphere

4.1 AUV Data processing

The analysis of the particular role of elastic wave scattering in the case of subcritical scattering from buried targets was triggered by some unexpected results produced by the synthetic aperture processing of the bistatic data collected by the AUV. Thus, for example, Fig. 5 shows the spectrogram of the timeseries obtained by beamforming over a 6.2 m synthetic aperture along the track, identified as number 25 in Fig. 2, focused on the nominal seabed position of the flush-buried sphere S2 [15]. This result clearly demonstrates that the maximum scattering from the target occurs at 10-12 kHz, in strong contrast to the much lower optimal frequency expected from traditional point-scatter modelling from simpler targets [11]. An initial arrival with a peak frequency at 5 kHz is evident as well, although at much weaker amplitude.

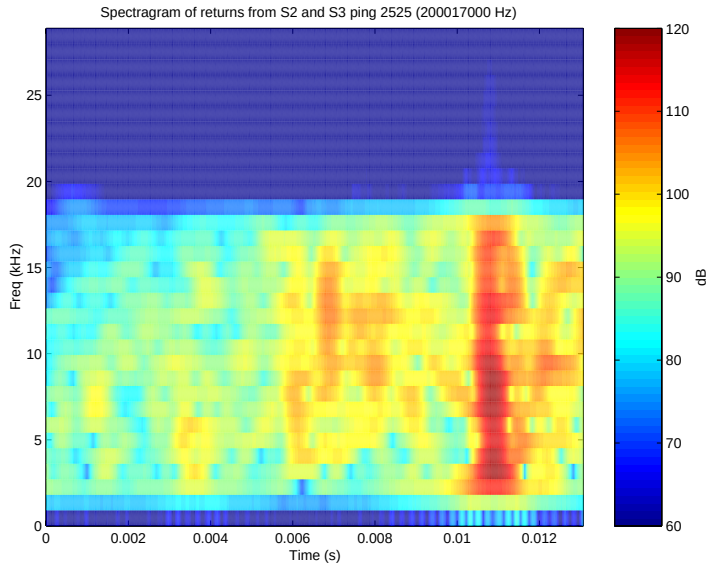

Figure 5 *The spectrogram of the beamformed time series for file 25 centred on S2. Clearly visible is the time frequency response of the flush buried sphere S2, between times of 6 and 8 ms. Below 8 kHz, S2 has one weak return at 6 ms, while in the 8-15 kHz range there are two distinct returns, the second of which is considered to be a membrane wave multipath of the sphere. The return from the proud sphere S3 is clearly visible at 10.5 ms.*

The parallel SAS imaging work of Edwards *et al*. [16], [17] has shown that in addition, the imaging shows the target to be displaced by approximately 1 m further away than its actual position, independently determined *in situ*.

These experimental findings lead to the hypothesis that the SAS imaging over the bistatic aperture was dominated by an elastic scattering component, rather than the expected 'specular' scattering of the evanescent, lateral wave. As shown in the following, the OASES-3D model supports this hypothesis, even though some discrepancies still exist and are the target of continued modelling and analysis effort.

4.2 OASES-3D Modelling

OASES-3D has been used to simulate the scattering from the target during mission x9814501 used in the analysis described above. The TOPAS source was positioned on a 10 m tall tower, 29.5 m from the target S2, which was insonified at 18.7° grazing angle, well below the critical angle independently estimated at 24° [7]. Micronavigation relative to the strong target S3 estimated the AUV track to be approximately perpendicular to the source-target axis, passing between the two at a distance of 3.8 m from S2 at the point of closest approach. The synthetic timeseries at 1 m spacing over a 10 m synthetic aperture are shown in Fig. 6(a). Figure 6(b) shows the spectrogram of the signal at the point of closest approach. The initial, strong arrival is the specular reflection of the incident lateral wave, appearing as a low-pass filtered replica of the 8 kHz Ricker wavelet emitted by the TOPAS, as expected. According to the spectrogram this arrival has a maximum at approximately 5 kHz. During the first approximately 1 ms following the specular scattering, a couple of arrivals are observed corresponding to the two first multiples of the longitudinal S_0 Lamb wave excited in the shell [18], following which a strong return appears on receivers close to the source-target axis in particular. This is the first 'flexural' shell wave, and as evidenced by the spectrogram, it has maximum frequency content at 10-12 kHz, with insignificant energy below 8 kHz. This frequency distribution contrasts to the one observed in the super-critical data, extensively investigated by Tesei *et al*. [18] which showed a maximum in the A_0 response at the 8 kHz coincidence frequency, with the subsonic A_{0-} and the supersonic A_{0+} modes dominating below and above the coincidence frequency, respectively.

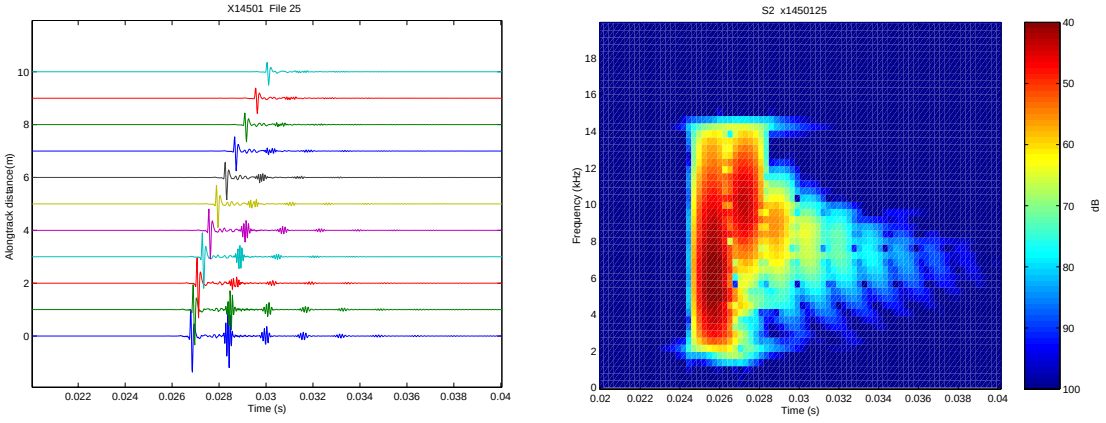

Figure 6 *OASES-3D synthetics of scattering from the flush-buried target S2 along a 10 m long synthetic aperture corresponding to the AUV track used for the SAS processing in Fig. 5(a) Synthetic time series at receivers spaced 1 m apart, with 0 m corresponding to a position on the source-target axis. (b) Spectrogram of timeseries at receiver position 0 m.*

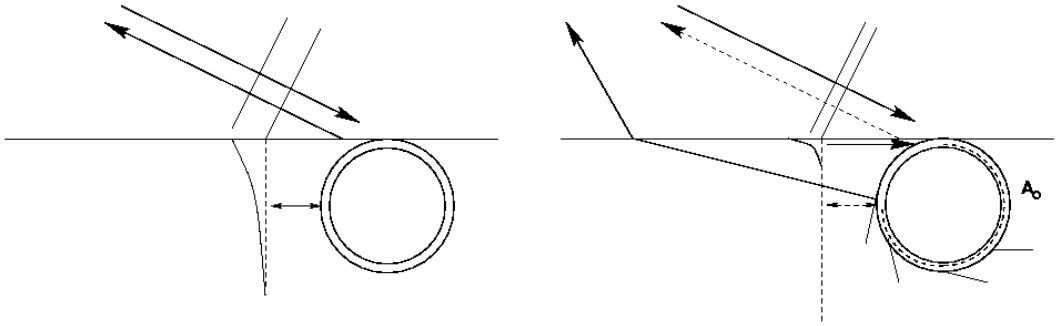

Figure 7 *Schematic representation of subcritical scattering from a flush-buried spherical shell. (a) At low frequencies the scattering is dominated by the specular scattering of the evanescent, lateral wave, with the back-scattering being excited by wave tunnelling. (b) At high frequencies the 'specular' component becomes insignificant because of the shallow penetration depth of the lateral wave, which, however, for shallow burial depth is sufficiently deep to couple efficiently into the 'flexural' A_0 Lamb waves, of which the supersonic A_{0+} component will radiate directly into the sediment, and transmit into the water column at super-critical angles.*

These results suggest that the physics of subcritical scattering from a flush-buried spherical shell is as sketched in Fig. 7. At low frequencies, Fig. 7(a), the back-scattering is dominated by the specular scattering of the evanescent, lateral wave. Thus, for a subcritical receiver the back-scattering is being excited by wave tunnelling, with an exponential decay with frequency as a result. In contrast, as illustrated in Fig. 7(b), at high frequencies the 'specular' component becomes insignificant because of the shallow penetration depth of the lateral wave. However, for shallow burial depth the target curvature near the seabed allows this evanescent 'tail' to couple efficiently into the 'flexural' A_0 Lamb waves, of which the supersonic A_{0+} component will radiate directly into the sediment. This radiated field will transmit into the water column at super-critical angles, even for receivers which are 'sub-critical' in a geometrical sense. Thus, the associated energy will arrive at water column receivers at angles ranging from vertical for a receiver above the target to the critical angle at distant receivers.

Consequently, for subcritical insonification the specular arrival will be low-pass filtered relative to the incident field while the flexural Lamb wave becomes high-pass filtered because of the more effective re-radiation into the sediment and back into the water column of the supersonic A_{0+} above the coincidence frequency. The multiples of the A_{0+} appear from the spectrogram to have decreasing peak frequency, which is explained by the linear frequency attenuation.

With this scattering physics, the same arrivals are predicted for a monostatic scenario, as evidenced by Fig. 8, which shows the corresponding synthetics for a 10 m horizontal aperture at the source range. The specular arrival is clearly significantly more low-pass filtered than in the bistatic case, which is expected because of the shallower receiver grazing angle. The A_{0+} arrival is decaying in amplitude as well due to increased geometrical spreading. Here it is interesting to note that this elastic arrival decays more rapidly with receiver offset than does the specular component. The reason for this is its longer path in the lossy sediment, for distant receivers corresponding to a path close to that of the head-wave.

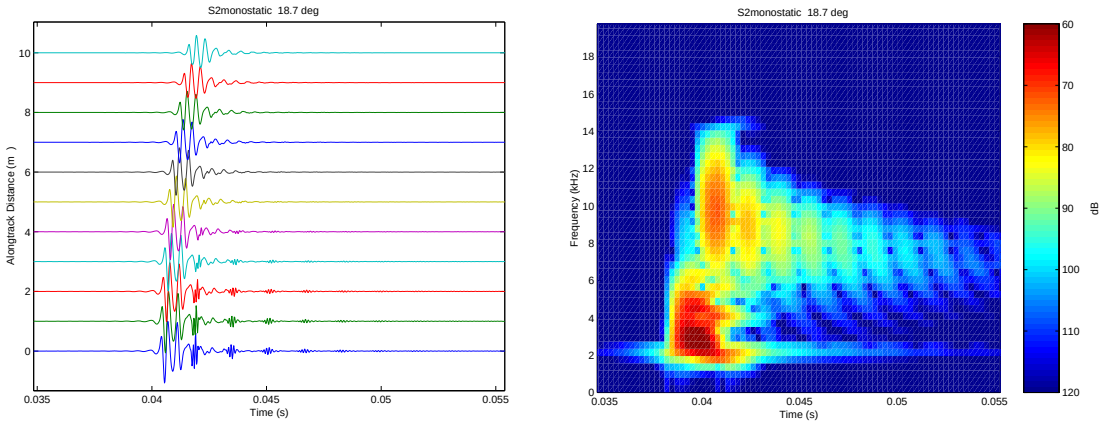

Figure 8 *OASES-3D synthetics of scattering from the flush-buried target for a 10 m long horizontal aperture at the source range. (a) Synthetic time series at receivers spaced 1 m apart, with 0 m corresponding to a position on the source-target axis. (b) Spectrogram of timeseries at receiver position 0 m.*

5. Discussion

The modelling and analysis of the GOATS'98 dataset described here has demonstrated that structural waves may provide efficient 'smoke-shifters' for completely buried targets, converting a subcritical, evanescent incident field into vertically propagating components which effectively couple back into the water column above the critical angle. The OASES-3D modelling framework has been used to show that such a mechanism is the likely cause for a strong delayed maximum observed in the bistatic scattering from a flush-buried spherical shell at frequencies an order of magnitude higher than predicted for simple point-targets at the same burial depth. The significance of such wavenumber conversion features of buried targets has strong implications for modelling. Thus, it is well established that for free floating targets or buried targets insonified above the critical angle, simple ray tracing, or plane wave methods, adequately describe the propagation to and from the targets, requiring only one wavenumber component for the incident field and one for the scattered field, determined by the source-target-receiver geometry. However, as demonstrated here, for subcritical insonification evanescent field components may be efficiently converted into vertically propagating components, and consequently requiring a spatial spectrum of finite width in the modelling.

In other words, the traditional plane-wave, ray-tracing approach to the propagation to and from the target is totally inadequate for evanescent excitation, and must be replaced by a scattering model incorporating a wide spatial spectrum of scattered propagation angles. The analysis also showed that although the structural scattering mechanisms also exist for monostatic geometries, their bistatic enhancement is much stronger than for the 'geometric', evanescent scattering. In addition, being due to the excitation of structural waves, the presence of this scattered component can potentially be applied for classification. This in turn suggests that the subcritical excitation of elastic waves in a flush-buried target may provide a bi-static enhancement significantly beyond that of the geometrically scattered component, which may be explored to increase coverage rate by bi- and multi-static configurations.

Even though the modelling presented here yields strong evidence for the significance of structural scattering in the evanescent regime there are some unexplained discrepancies

remaining. Thus, the model appears to overestimate the specular, geometric component, compared to the experiment, and the time separation between the geometric and structural arrivals are not correctly predicted. The reason may be that multiple scattering effects are significant in reducing the geometric arrival to insignificance, such that the initial observed arrival is instead an S_0 arrival, a hypothesis which is the target of continued analysis and modelling effort.

Acknowledgements

The author appreciates the effort of the large number of people who made the GOATS'98 experiment a success. In that regard a special appreciation of the extremely enjoyable collaboration with Edoardo Bovio and Alain Maguer in designing and executing the experiment. Alain is not only a world class experimentalist, but he also fearlessly jumped into the ocean to save the AUV and the day! Alain had excellent support by Warren Fox and Per Arne Sletner in running the TOPAS source facility from the shore laboratory at Marciana Marina. Thanks to Bruno Miaschi and Alberto Figoli for an outstanding job designing and building the AUV array and acquisition system, and to Reg Hollett for developing the data acquisition software and interfacing it with the AUV control. Piero Guerrini pulled it all together as Engineering Coordinator. The outstanding effort of the crews of R/V *Alliance* and T/B Manning is highly appreciated, as is the superb job of Bob Grieve and Brad Moran of the MIT Sea Grant AUV Laboratory operating the Odyssey II class 'Xanthos' AUV. A special thanks to the Management at SACLANTCEN for squeezing GOATS'98 into their programme of work on short notice and for their continued support for the entire project. Finally, the support of the Office of Naval Research, in particular the 'GOATS team' of Program Managers: Jeff Simmen, Tom Curtin, Tom Swean, Randy Jacobson, and Bruce Johnson, is highly appreciated.

References

[1] Schmidt, H., Lee, J. Physics of 3-d scattering from rippled seabeds and buried targets in shallow water. *Journal of the Acoustical Society of America*, **105**, 1999:1605-1617.

[2] Boulinguez, D., Quinquis, A. Underwater buried object recognition using wavelet packets and fourier descriptors. *In*: Proceedings of the 10th International Conference on Image Analysis and Processing, pp 478-83, Los Alamitos, CA, 1999. IEEE Computing Society.

[3] Roitblat, H.L., Au, W.W.L., Nachtigall, P.E., Shizumura, R., Moons, G. Sonar recognition of targets embedded in sediment. *Neural Networks*, **8**, 1995:1263-73.

[4] Simpson, H.J., Houston, B.H., Frederickson, C.K., Lim, R. Measurements and analysis of scattering from proud and buried targets in a shallow-water laboratory environment. *In*: MTS/IEEE Oceans'99 Conference Proceedings: Riding the Crest into the 21st Century, volume 3, pp 1154-7, Piscataway, NJ, 1999.

[5] O'Neill, K. Broadband bistatic coherent and incoherent detection of buried objects beneath randomly rough surfaces. *IEEE Transactions on Geoscience and Remote Sensing*, **38**, 2000:891-8.

[6] Scott, W.R. Jr., Martin, J.S., Larson, G.D. Investigation of a technique that uses elastic waves to detect buried land mines. *In*: Proceedings of the IEEE 2000 International Geoscience and Remote Sensing Symposium, volume 4, pp 1640-2, Piscataway, NJ, 2000.

[7] Maguer, A., Fox, W.L.J., Schmidt, H., Pouliquen, E., Bovio, E.. Mechanisms for subcritical penetration into a sandy bottom: experimental and modelling results. *Journal of the Acoustical Society of America*, **107**, 2000.

[8] Ingenito, F. Scattering from objects in a stratified medium. *Journal of the Acoustical Society of America*, **82**, 1987:2051-2069.

[9] Makris, N.C. A spectral approach to 3-d object scattering in layered media applied to scattering from submerged spheres. *Journal of the Acoustical Society of America,* **104**, 1998:2105-2113.

[10] Fawcett, J. Finite element modelling of three-dimensional scattering from azimuthally-symmetric elastic shells. SACLANTCEN SR 273, 1998.

[11] Schmidt, H., Lee, J. Physics of 3-D scattering from rippled seabeds and buried targets in shallow water. *Journal of the Acoustical Society of America,* **105,** 1999:1605-1617.

[12] Jensen, F., Kuperman, W.A., Porter, M.B., Schmidt, H.. Computational Ocean Acoustics. AIP Press, New York, 1994.

[13] Schmidt, H., Glattetre, J.. A fast field model for three-dimensional wave propagation in stratified environments based on the global matrix method. *Journal of the Acoustical Society of America,* **78,** 1985:2105-2114.

[14] Fawcett, J.A. Scattering from an elastic cylinder buried beneath a rough water/basement interface. *In*: Pace, N.G., Pouliquen, E., Bergem, O., Lyons, A.P., *editors*. High Frequency Acoustics in Shallow Water. SACLANTCEN CP-45, 1997.

[15] LePage, K.D., Schmidt, H. Bistatic synthetic aperture imaging of proud and buried targets from and auv. *In*: Proceedings, GOATS 2000 Conference. SACLANTCEN CP-46, 2001.

[16] Edwards, J.R., Schmidt, H., LePage, K.D. Bistatic synthetic aperture target detection and imaging with an AUV. *IEEE Journal of Oceanic Engineering*, 2001.

[17] Edwards, J.R., Schmidt, H., LePage, K.D. Synthetic aperture processing of GOATS'98 bistatic acoustic data. *In*: Proceedings, GOATS 2000 Conference. SACLANTCEN CP-46, 2001.

[18] Tesei, A., Lim, R., Maguer, A., Fox, W.L.J., Schmidt, H. Measurements of acoustic scattering from partially and completely buried spherical shells. *Journal of the Acoustical Society of America* Submitted, 2001.